

## Adaptive higher-order submodular potentials for pulmonary artery-vein segmentation

Yoshiro Kitamura<sup>1</sup>, Yuanzhong Li<sup>1</sup>, Wataru Ito<sup>1</sup>, Hiroshi Ishikawa<sup>2</sup>

<sup>1</sup> Imaging technology center, Fujifilm corporation, Minato, Tokyo, Japan

<sup>2</sup> Department of computer science and engineering, Waseda university, Shinjuku, Tokyo, Japan

**Abstract.** We propose a novel method of 3D segmentation based on Conditional random field that utilizes higher-order potentials. We introduce higher-order terms into the energy that encourage sets of voxels to be entirely in one segment or the other. The set can for instance be of those voxels on a smooth curve, which we use for segmenting pulmonary vessels that is known to run in an almost straight line. The higher-order terms are of a special kind that can be converted to submodular first-order terms, which can then be minimized globally using graph cuts. We also determine the weight of these terms, or the degree of the aforementioned encouragement, in a principled way by learning from training data with the ground truth. We show the effectiveness of the method in an application to fully-automatic pulmonary artery-vein segmentation in 3D CT images, which is hard as the artery and the vein often entwine each other in the lung. The method is an important step for diagnosis and/or surgery simulation of lung cancer.

Keywords: Graph cuts, Higher-order function, Artery-vein segmentation

### 1 Introduction

Lung cancer is the most common cause of cancer-related deaths in the world [1]. However, thanks to the multi-detector CT, which has become common in clinical practice, lung cancers can now be detected in early stages. Then, minimally invasive surgery such as lobectomy or segmentectomy can be performed [2]. This surgery requires a precise knowledge of the anatomy of patient's pulmonary vessels and bronchi, where pre-surgery simulation and navigation systems have a great clinical importance. These systems in turn require that each organ is segmented in the CT images. Since manual segmentation is too time consuming, fully automatic segmentation of pulmonary artery and vein is the key to such systems.

There are not many methods suitable for segmenting arteries and veins, which is difficult as they often entwine each other in the lung. A preliminary study [3] was reported which utilized an algorithm based on region growing. In [4], a fast-marching algorithm that propagates a front in the direction of minimal cost was used to segment the main pulmonary arteries. Another method [5] combines the fuzzy distance transform and morphologic features. These methods require the user to provide seed

points. A fully automatic approach [6] utilizes the specific anatomical knowledge that a pulmonary artery is often in close proximity of an airway, going in parallel.

In this paper, we propose a novel segmentation method based on the Conditional Random Field (CRF) framework. The method utilizes higher-order submodular potentials which allow modeling complex anatomy such as the pulmonary vessels.

## 2 Theory and Method

The segmentation problem can be formulated as a voxel-labeling problem. Many conventional methods use the Markov random field model that minimizes the energy function with unary and pairwise terms:

$$E(X) = \sum_{a \in V} \theta_a(x_a) + \sum_{a \in V, b \in N_a} \theta_{ab}(x_a, x_b), \quad (1)$$

where  $X$  is the vector of binary variables  $x \in \{0, 1\}$  indexed by the set  $V$  of voxels, and  $N_a$  is the set of voxels in the neighborhood of voxel  $a$ . The functions  $\theta_a$  and  $\theta_{ab}$  give the potential for the binary label  $x_a$  and the label pair  $(x_a, x_b)$ , respectively.

### 2.1 Pseudo-Boolean Functions and Order reduction technique

Pseudo-boolean functions such as (1) can always be written as a polynomial, e.g.,

$$\theta_{ab}(x_a, x_b) = \theta_{ab}(0, 0)(1-x_a)(1-x_b) + \theta_{ab}(0, 1)(1-x_a)x_b + \theta_{ab}(1, 0)x_a(1-x_b) + \theta_{ab}(1, 1)x_ax_b.$$

In this quadratic polynomial form, if all of the weights of the quadratic terms in an energy function are negative, it is *submodular* and can be globally minimized by the graph-cut algorithm in polynomial time [7]. Otherwise, non-submodular functions can be optimized by the Quadratic Pseudo Boolean Optimization (QPBO) algorithm [8].

Recent advancements enable us to utilize higher-order energy functions, which contain, in the polynomial form, terms of higher degree than two. According to [9], a higher-order pseudo-boolean function can be transformed into an equivalent first-order (quadratic) function by adding auxiliary variables. Then the original problem can be solved by minimizing the transformed function by conventional algorithms such as graph cuts or QPBO.

Submodular energy functions have great advantages since they can always be minimized globally in polynomial time using graph cuts. Thus, higher-order functions that are converted to submodular quadratic functions are of special interest. Two such cases are known [9, 10]:

$$-x_1x_2\dots x_n = \min_{z \in \{0,1\}} -z(x_1 + x_2 + \dots + x_n - (n-1)), \quad (2)$$

$$-(1-x_1)(1-x_2)\dots(1-x_n) = \min_{z \in \{0,1\}} z(x_1 + x_2 + \dots + x_n - 1), \quad (3)$$

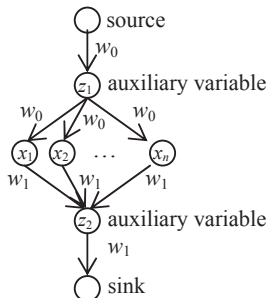


**Fig. 1.** The graph construction of the function:  
 $-w_0(1-x_1)(1-x_2)\dots(1-x_n) - w_1x_1x_2\dots x_n$

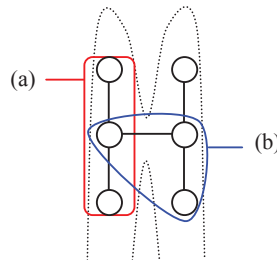


**Fig. 2.** Artery and vein model in which the two are in contact at the middle point

where  $z \in \{0, 1\}$  is the auxiliary variable and  $n$  is the degree of the function. Note that the RHS of the transformations are submodular functions (i.e., those with which the coefficients of all quadratic terms are negative) inside a minimization. Adding the higher-degree terms on the left hand side to a minimization problem is equivalent to adding the quadratic terms on the right hand side and adding the auxiliary variable  $z$  to the set of variables over which to minimize. In terms of graph-cut construction, they correspond to the graphs illustrated in Fig. 1. Note that these transformations are called the  $P^n$ -Potts model in [10].

**2.2 Adaptively-selected Potts potential**

We introduce a novel use of higher-order submodular functions, which we call the *adaptively-selected Potts* potentials, in segmentation. The idea is to add the higher-order terms of the form (2) and (3) to encourage all of the  $n$  variables in the term to have the same value (0 or 1). For instance, both sides in equation (2) are  $-1$  if and only if all the variables  $x_1, \dots, x_n$  are 1, and 0 otherwise. By choosing the variables (i.e., voxels) to include in such higher terms, we can encourage specific configurations of many variables, while keeping the energy submodular. In other words, we can determine how much the voxel set is prone to being in the same segment. For instance, we can encourage voxels forming a curve with low total curvature to be in the same segment as follows. Consider a segmentation problem of separating the artery and vein branches in Fig. 2, which is difficult using a first-order energy (1) as the two vessels are in contact at the middle. Since the pulmonary vessels are known to run in an almost straight line in the lung, we can encourage the set (a) of voxels on a straight line more than (b) that forms a right angle by adding a term of the form (2) or (3) or both to the energy, with the variables corresponding to the voxels in (a). Of course, we can also control how much we encourage this by multiplying the term by a positive number of varying magnitude. Note we can have any number of voxels in the set, though in the example there are only three.

The crucial aspect of the method is that we choose which set of voxels to add in a principled way, adapting to the given data. We illustrate this process in the case of the segmentation problem of pulmonary artery and vein in the following sections.

### 3 Pulmonary artery-vein segmentation

We present a fully-automatic segmentation method from chest CT Angiography data to evaluate the proposed method. The CTA data was acquired after injecting contrast agents into patients. Therefore, the contrast of arteries and veins had been enhanced from their roots to the peripheral branches. The segmentation method consists of the three steps: root position detection, vessel region extraction, and artery-vein segmentation. Schematic images of the steps are shown in Fig. 3.

**Root position detection.** The root positions correspond to the pulmonary artery trunk and the left atrium of the heart. These are detected by landmark detectors [11]. Two types of appearances on axial images were learned from training data by using a machine learning method [12].

**Vessel region extraction.** The vessel regions are segmented by the conventional graph-cut method which utilizes unary and pairwise potential [7]. Pulmonary vessels have different characteristics in the mediastinum and the lung. The thick vessels in the mediastinum are extracted as continuously extending regions from the detected root positions. To do this, foreground seeds (unary terms) are set around voxels where the roots are detected. Background seeds are given to voxels having lower intensity than the root positions, and are also given at the bronchus wall regions extracted by the bronchus extraction method in [13]. Because bronchi are often in contact with pulmonary vessel trunks, these regions need to be removed from the vessel region. The pairwise terms smooth the labeling depending on the gradient values of the image. While the vessels having tubular appearances in the lung are detected by the multi-scale vessel detector [14] based on machine learning. The detected candidates are provided as foreground seeds to the graph-cut method. The background seeds and the pairwise terms are set in a similar way. Finally, binary segmentation of the vessels is obtained.

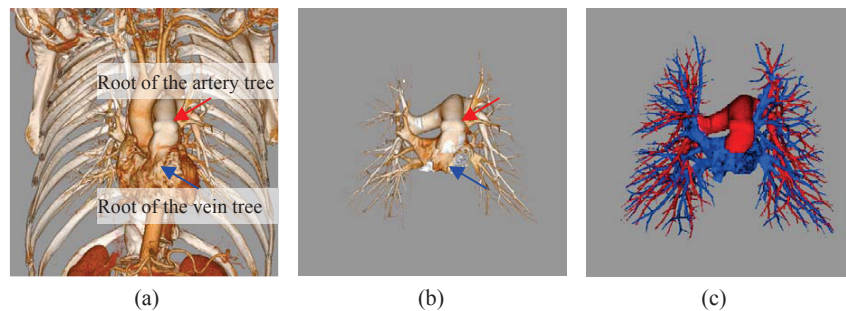


**Fig. 3.** Schematic images of the pulmonary artery-vein segmentation method. The method consists of the three steps: (a) root position detection, (b) vessel region extraction, and (c) artery-vein segmentation.

**Artery-vein separation.** Given the root positions and the vessel regions, the third step separates the vessel regions into pulmonary artery (PA) and pulmonary vein (PV). The energy function consists of unary, pairwise, and the higher-order terms:

$$E(X) = \sum_{a \in V} \theta_a(x_a) + \sum_{a \in V, b \in N_a} \theta_{ab}(x_a, x_b) + \sum_{c \in C} \theta_c(X_c), \quad (4)$$

where  $c$  is the *clique* (the set of voxels) for adaptively-selected Potts potential  $\theta_c(X_c)$ , which is of the form  $-w_c \prod_{a \in c} x_a$  or  $-w_c \prod_{a \in c} (1 - x_a)$  (corresponding to (2) or (3)) with positive weight  $w_c$ .  $C$  is the set of cliques and  $X_c$  stands for the set  $\{x_a \mid a \in c\}$  of variables. The unary terms are set around the root positions to force the voxels there to be labeled appropriately. The pairwise terms smooth the labeling to different degrees depending on the gradient values of the image and the plateness measure calculated by Hessian analysis [15] to emphasize boundaries where the artery and the vein are in contact. These weights were determined heuristically.

### 3.1 Implementation details of the adaptively-selected Potts potential

In this section, we describe how the set  $C$  of cliques in (4) and the weight  $w_c$  for each higher-order term  $\theta_c(X_c)$  are determined in a principled way in the case of the pulmonary artery-vein segmentation problem. Notwithstanding the strong tendency of the pulmonary vessels to run straight, they of course do not always run in a completely straight line; they sometimes curve or branch. To allow for such flexibility, we encourage sets of voxels according to the curvature of the curve segment they form.

First, to choose the curve segments, we utilize a shortest path algorithm. At each voxel position, a shortest path tree is constructed from the local region, which covers 15 voxel lengths in diameter, with the 26-voxel neighborhood topology. Each edge is given a weight depending on voxel intensities. Then the minimum cost path of about 15 voxel length is selected from the tree. The chosen path is a clique  $c$  in (4) and the degree of the higher-order potential  $\theta_c(X_c)$  is the number of the voxels therein. Thus, one higher order term per voxel is added by finding the best segment. Here, the length of the path should be larger than the diameter of the vessel so that we can estimate the direction of the vessel.

Next, we set the weight  $w_c$  for the higher-order potential, determining how much we encourage the curve segment to be entirely in one of the segments (artery or vein). Here, we consider only two cases: all labels are the same or not, whether it is artery or vein, because there are little difference between their appearances. This corresponds to giving the same weight for the terms in eq. (2) and (3). The probabilities of the two cases are learned from the reference segmentation data that was manually prepared. For each path, several features are calculated from the voxel set: the features include the length of the path, the straight-line distance between the two endpoints, the total curvature along the path, the maximum curvature on the path, the maximum intensity derivative, and the variance of the intensity derivative. (Fig. 4 illustrates two examples of the selected paths. Comparing Fig. 4 (a) with (b), the straight-line distance

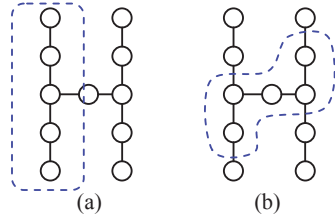


Fig. 4. Examples of the selected paths

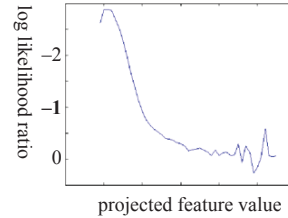


Fig. 5. Graph of learned log likelihood ratio

between the two endpoints in (a) is larger than in (b), and the total curvature along the path in (b) is larger than in (a).) Then, for each of the two cases (all the voxels on the path have the same label or not), the histogram for the feature values are generated and the log likelihood ratio of their probabilities:  $-\log(\Pr(\text{not all same}) / \Pr(\text{all same}))$  is learned. To learn the likelihood ratio from the limited number of samples, the feature vectors were projected to one dimension using Linear Discriminant Analysis before learning. Fig. 5 shows the graph of the learned log likelihood ratio for the projected feature value. The likelihood value corresponding to the feature value for given data is directly used as the weight of the adaptively-selected Potts potential. Note that the weight  $-w_c$  of the energy is clipped to zero when it is positive in order to keep the potential submodular.

Snapshots of selected segments for the adaptively-selected Potts potentials are shown in Fig. 6. Each segment is drawn in green through the selected voxels. The brightness indicates the likelihood: the higher the likelihood of the segment is, the brighter it is drawn.

### 3.2 Experimental Validation

For validation, we used ten chest CT Angiography images that were not used for learning. Ground truth data were prepared for these images by manually labeling the artery and vein regions. Note that the ground truth data was established only for ves-

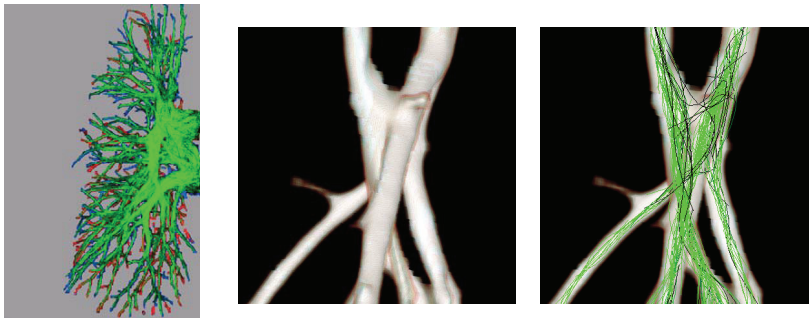
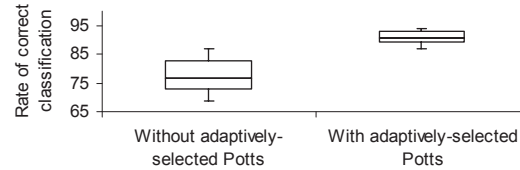


Fig. 6. Snapshots of set adaptively-selected Potts potential. Each green filament represents a higher order clique. The potential weight for the clique is determined according to its shape: the higher the weight is, the brighter it is drawn.



**Fig. 7.** Plots of correct classification rates comparing methods with and without the adaptively-selected Potts potential

sels with CT values more than -200 HU in the lungs. Even under this condition, we think this ground truth data is sufficient to validate artery-vein separation, since it covers most important vessels except for peripheral branches which are not often in contact with other vessels. The artery and vein centerlines were generated by thinning operation of the labeled regions. Classification accuracies were calculated as the percentages of the length that the vessel in the ground truth was correctly classified in the segmentation results. Miss-extraction rates were also calculated as the percentages of the vessel that was not segmented as artery or vein.

We compared the extraction results obtained by the energy functions with and without the adaptively-selected Potts potential. All steps were executed automatically without any user interaction. To summarize the evaluation results, the average rates of correct classification were 90.7% in the case with the adaptively-selected Potts potential, and 77.5% in the case without. The average miss-extraction rate which was common between both methods was 3.3%. The box plot of the results is shown in Fig. 7. Fig. 8 is an example of the case that a major difference was seen between the two methods. The method without the adaptively-selected Potts potential generated a large misclassified region, as it used only the pairwise term as a typical conventional method does. Such a method tends to fail to separate regions that are in contact over a large area or with an unclear boundary (Fig. 8 (c)). The case where even the method without the adaptively-selected Potts potential achieved a high rate of correct classification is shown in Fig. 9. In this case, the difference of intensity values between the artery and the vein were comparably higher due to the timing of the injection of the contrast agents (Fig. 9 (c)). However, the method with the adaptively-selected Potts potential obtained a higher rate, correctly classifying more vessels around the peripheral.

In this experiment, we assumed that there was no difference in appearance between the artery and the vein. However, it is known that an artery often goes along an airway [6]. It is an interesting future line of research to consider different weights of the adaptively-selected Potts potential for the artery and the vein depending on the proximity to the airways. More generally, using the adaptively-selected Potts potential for other shapes such as plate-like or arc-like structures is likely to improve the segmentation accuracy of other kinds of objects.

## 4 Conclusion

We proposed a novel segmentation method that utilizes higher-order submodular functions which allow modeling complex anatomy such as the pulmonary vessels. The higher-order terms encourage sets of voxels to be entirely in one segment or the other, and the energy with them is still submodular so that it can be globally minimized. The degree of encouragement is learned from example data with the ground truth. Experimental validation of the proposed method for pulmonary artery-vein segmentation showed a clear efficacy of this method. We consider this method applicable to various other segmentation problems.

## References

1. J. Ferlay, H. R. Shin, F. Bray, D. Forman, C. Mathers, D. M. Parkin, : Estimates of world-wide burden of cancer in 2008: GLOBOCAN 2008, *Int J Cancer*, vol. 127, no. 12, pp. 2893–2917 (2010)
2. N. Ikeda, A. Yoshimura, M. Hagiwara, S. Akata, H. Saji, : Three dimensional computed tomography lung modeling is useful in simulation and navigation of lung cancer surgery, *Ann Thorac Cardiovasc Surg* (2013)
3. T. Yamaguchi, T. Kitasaka, K. Mori, Y. Mekada, J. Hasegawa, J. Toriwaki, H. Otsuji, : A preliminary study for automated recognition of branches of pulmonary artery and vein using anatomical positional relations from a 3-D chest X-ray CT image, *CARS2002*, pp. 782–787 (2002)
4. R. Sebbe, B. Gosselin, E. Coche, B. Macq, : Pulmonary Arteries Segmentation and Feature Extraction through Slice Marching. In *Proc. ProRISC workshop on Circuits, Systems and Signal Processing*, (2003)
5. P. K. Saha, Z. Gao, S. K. Alford, M. Sonka, E. A. Hoffman, : Topomorphologic separation of fused isointensity objects via multiscale opening: separating arteries and veins in 3-D pulmonary CT, *IEEE Trans. Medical Imaging*, 29, (2010).
6. Y. Mekada, S. Nakamura, I. Ide, H. Murase, H. Otsuji, : Pulmonary Artery and Vein Classification using Spatial Arrangement Features from X-ray CT Images, *Proc. APCCM2006*, pp. 232-235 (2006)
7. Y. Boykov, V. Kolmogorov, : An Experimental Comparison of Min-Cut/Max-Flow Algorithms for Energy Minimization in Vision, *IEEE PAMI*, 26(9), 1124-1137, (2004)
8. C. Rother, V. Kolmogorov, V. Lempitsky, and M. Szummer, : Optimizing Binary MRFs via Extended Roof Duality, *Proc. IEEE CS Conf. Computer Vision and Pattern Recognition*, (2007)
9. H. Ishikawa, : Transformation of General Binary MRF Minimization to the First Order Case, *IEEE Trans. PAMI*, vol. 33, no. 6, pp. 1234-1249, (2011)
10. P. Kohli, M. P. Kumar, P. H. S. Torr, : P3 & Beyond: Move making algorithms for solving higher order functions, *IEEE Trans. PAMI*, vol. 31 no. 9, pp. 1645-56, (2009)
11. C. Wang, Y. Li, W. Ito, K. Shimura, K. Abe, : A machine learning approach to extract spinal column centerline from three-dimensional CT data, *Proc. SPIE MI*, 72594T, (2009)
12. J. Friedman, T. Hastie, R. Tibshirani, : Additive logistic regression: a statistical view of boosting (with discussion and a rejoinder by the authors), *Annals of Statistics*, 28(2), pp. 337–407, (2000)

13. T. Inoue, Y. Kitamura, Y. Li, W. Ito,: Robust airway extraction based on machine learning and minimum spanning tree, Proc. SPIE MI, 86700L, (2013)
14. Y. Kitamura, Y. Li, W. Ito,: Automatic coronary extraction by supervised detection and shape matching, Proc. IEEE ISBI, pp. 234-237 (2012)
15. A. F. Frangi, W. J. Niessen, K. L. Vincken, M. A. Viergever,: Multiscale vessel enhancement filtering, Proc. MICCAI, vol. 1496, pp. 130-137 (1988)

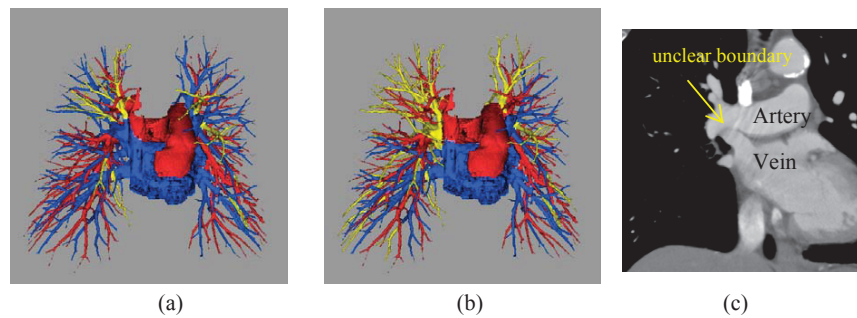


**Fig. 8.** The segmentation results of the case that the artery and the vein are in contact over a large area and with an unclear boundary. (a) was obtained from the method with adaptively-selected Potts potential, and (b) the method without. The red and blue regions represent artery and vein, respectively. The yellow represents misclassified regions. (c) is a coronal image around the pulmonary hilum.

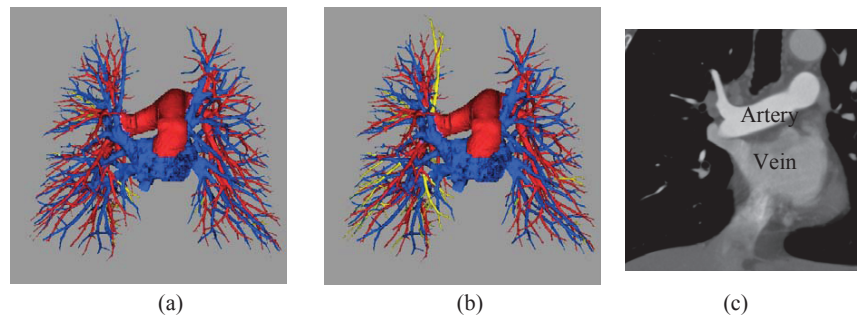


**Fig. 9.** The segmentation results of the case that the difference of intensity values between the artery and the vein were comparably higher. (a) was obtained from the method with adaptively-selected Potts potential, and (b) the method without. The red and blue regions represent artery and vein, respectively. The yellow represents misclassified regions. (c) is a coronal image around the pulmonary hilum.